Proceedings of ASME HTFED04:
2004 ASME Heat Transfer/Fluids Engineering Summer Conference
July 11-15, 2004, Charlotte, North Carolina, USA

HT-FED2004-56825

AN EXPERIMENTAL STUDY OF SYNTHETIC JETS FROM RECTANGULAR ORIFICES

Ivana M. Milanovic
University of Hartford
West Hartford, CT 06117

Khairul B. M. Q. Zaman
NASA Glenn Research Center
Cleveland, OH 44135

ABSTRACT

Results of an experimental investigation on isolated synthetic jets in crossflow from rectangular orifices of different aspect ratio and orientation are presented. Three aspect ratios, AR = 4, 8, and 16, with pitch α = 90°, were investigated. Additionally, the AR = 8 case was pitched at 20°. The yaw angle, β, was varied through 0°, 10°, 45° and 90°. All orifices had same exit area and the data were compared with synthetic as well as steady jet from a circular orifice of same area. Hot-wire measurements were performed to obtain all three components of mean velocity and turbulent stresses. Data were acquired for momentum-flux ratio up to J = 50. Distributions of time- and phase-averaged data were obtained on the cross sectional plane at x/D = 0.5, 5 and 10, as well as on the axial plane of the symmetry.

Qualitative flowfield similarity between synthetic and steady jets is observed. However, high-momentum 'cap' above the low-momentum 'dome', characteristic of steady jets, does not necessarily appear in the synthetic jet. The position and shape of the high-momentum region depend on the distance from the orifice, pitch, yaw as well as momentum-flux ratio. Consequently, the location of the minimum velocity in the 'dome' measured at the plane of symmetry, y_{min}, is adopted as a reference for penetration estimate and trajectory comparison. For AR = 16, the dome is the largest in area with maximum velocity deficit. However, the penetration is somewhat higher for AR = 4. Increase in yaw reduces the spatial extent of the dome and the penetration height but augments the velocity deficit.

At low J the dome is connected to the boundary layer and traces of the cap of high momentum fluid are visible above it. Increase in J lifts the dome and reorganizes the high-momentum fluid around its perimeter, eventually bringing it underneath. Phase-averaged data document dynamic topological changes within the cycle. Phase-averaged streamwise velocity contours on the cross-sectional plane exhibit behavior commensurate with that seen in time-averaged data at various J.

Keywords: synthetic jets, crossflow, rectangular orifices, flow control, mixing.

NOMENCLATURE

A	Root-mean-square (r.m.s.) voltage input to loudspeaker
AR	Aspect ratio
D	Equivalent diameter of orifice based on area
f	Forcing frequency
h	Orifice height (or width)
J	Momentum-flux ratio, $J=\left(V_{max}/U_\infty\right)^2$ for synthetic, and $J=\left(U_j/U_\infty\right)^2$ for steady jets
L_0	Stroke length, $L_0=\int_0^{T/2} v_0(t)\,dt$
Re	Reynolds number, $Re=\bar{V}D/\nu$, $\bar{V}=2V_0$
t	Time
T	Forcing period, $T=1/f$
V_0	Velocity during discharge phase of the cycle averaged over entire period, $V_0=\frac{L_0}{T}=f\int_0^{T/2} v_0(t)\,dt$
$\bar{V}$	Average velocity during discharge phase of the cycle ($=2V_0$)
V_{max}	Maximum velocity during discharge phase
VR	Velocity ratio, $VR=U_j/U_\infty$
$v_0(t)$	Velocity at exit center of orifice (at $x=y=z=0$)
U, V, W	Mean velocity in streamwise, normal and spanwise directions
u', v', w'	Turbulence intensities in streamwise, normal and spanwise directions
w	Orifice length

x, y, z Cartesian coordinates in streamwise, normal and spanwise directions (Fig. 1)

α Jet pitch angle, between orifice axis and test section floor

β Jet yaw angle, between orifice major axis and crossflow direction

Subscripts

j Jet

∞ Freestream

INTRODUCTION

The interaction between a jet and a crossflow produces complex flowfield topology that is relevant to a variety of technologically important applications. Jets in crossflow (JICF) are utilized for separation prevention, virtual aeroshaping, mixing and heat transfer enhancement, thrust vectoring as well as noise control. Investigation of JICF dates back to 1950s when it was observed [1] that an inclined jet produces a vortex system similar to one from a wing-type vortex-generator. In an effort to find an alternative to solid vortex generators for flow control purposes steady jets at different pitch and yaw angles were studied over a range of velocity ratios [2-8]. However, additional working fluid and hardware requirements put considerable constraints on the use of JICF. In recent research synthetic or zero-net-mass-flux jets [9-15] have emerged as a promising means of flow control.

A synthetic jet is formed from the ambient fluid driven by fluctuating pressure. It may be produced by a cavity-orifice configuration with a vibrating membrane facing the orifice. Forced motion of the membrane results in a periodic discharge/suction through the orifice. Ambient fluid is entrained into the cavity during the suction. Subsequent discharge is characterized with an acceleration of the slug of fluid in the orifice, separation at the sharp edges, and entrainment of the surrounding fluid into the vortical structure. Self induction propels the vortex away from the orifice. Consequently, the synthetic jet is generated by a train of discrete vortices that, after a few orifice diameters downstream, resembles a continuous jet.

Smith and Glezer [9] investigated isolated synthetic jets issuing from a slot with aspect ratio AR = 150. Increased entrainment and development to self-similarity closer to the orifice was noted, in comparison with steady jet. Smith and Swift [14] also showed that synthetic jets (AR = 30) in the near field grow more rapidly both in width and volume flux due to the presence of vigorous vortical structures. Smith [16] explored the interaction among an array of synthetic jets exiting from rectangular orifices (AR = 45) with turbulent boundary layer, at J = 1.44. In the "streamwise configuration" where major axes were aligned with the cross-flow (β = 0 deg) the velocity profiles were similar to those measured in a JICF. The jet trajectory for the "spanwise array" (β = 90 deg) was found to follow the power law of a JICF. Bridges and Smith [17] investigated the interaction between a synthetic jet and a turbulent boundary layer while varying the orientation of a rectangular orifice (AR = 98). Data for yaw angles of 0, 10 and 20 deg, were obtained at the momentum-flux ratio of J = 0.67. Increased turbulence intensity in the boundary layer was observed for non-zero yaws. Vortical structure inferred from mean velocity contours was also found to depend on the yaw.

It is evident that numerous fundamental and applied studies have been conducted in the area of synthetic jets issuing from rectangular orifices both with and without the crossflow. However, they are mostly focused on high aspect ratio configurations with low-speed discharge and small momentum-flux ratios. The effects of varying aspect ratio, higher Reynolds numbers and momentum-flux ratio have not been fully explored. Detailed flowfield data including vorticity and turbulent stresses are in demand by code developers. This provided the motivation for the current work.

The present experimental investigation on isolated synthetic jets in the crossflow (SJCF) was conducted in a low-speed wind tunnel with hot-wire anemometry. Synthetic jets, produced by a cavity-membrane arrangement, issued into the crossflow from rectangular orifices of different aspect ratio and orientation. Time- and phase-averaged measurements were conducted for various configurations.

EXPERIMENTAL SETUP

The experiments were conducted in a NASA Glenn Research Center open-circuit low-speed wind tunnel with 30 in. (760 mm) wide x 20 in. (510 mm) high test section. Synthetic jets were created by a loudspeaker (Altec Lansing 37 cm woofer) housed in a chamber underneath the test section. The rectangular orifices were cut in a 10 in. (254 mm) diameter by 0.5 in. (12.7 mm) thick clear plastic plate. The disc was mounted flush on the test section floor and placed centrally near the beginning of the test section. The set–up is shown schematically in Fig. 1. Rectangular orifices were of aspect ratio AR = 4, 8 and 16. All configurations had the same equivalent diameter based on the exit cross-sectional area, D = 0.75 in. (19 mm). The pitch angle, α, measured between the nozzle centerline and the floor of the test section was 90 deg for most cases. Additionally, an orifice with AR = 8 was set at α = 20 deg. The orifice plate could be rotated to vary the yaw angle, β, measured between the nozzle major axis and the direction of the crossflow. For the AR = 8 case, four yaw angles, 0, 10, 45 and 90 deg. were investigated.

The data acquisition on a cross-sectional plane of the SJCF at various streamwise locations was performed using two adjacent x-film probes (TSI 1241-20), one placed in 'u-v' and the other in 'u-w' orientation. The probes were traversed under automated computer control through the same grid points allowing the measurement of all three components of mean velocity and turbulence intensity. The details of the probe calibration and uncertainty estimates can be found in Ref. 8. The origin of the coordinate system is located at the center of the orifice as illustrated in Fig. 1. The streamwise (i.e.

crossflow) direction is denoted by x, the direction normal to the tunnel floor is denoted by y, and the spanwise direction by z. The Helmholtz resonance frequency for the cavity-orifice was about 33 Hz. Most measurements were carried out at this resonant frequency and a constant crossflow velocity of U_∞ = 22.8 ft/s (6.95 m/s). The approach boundary layer was turbulent with a thickness of about 0.4 D. The input signal to the loudspeaker was a sine wave and the characteristics of the oscillatory flow at the orifice exit were first surveyed with a single hot-wire. The amplitude was controlled by varying the input voltage, A.

RESULTS AND DISCUSSION

As stated earlier, governing parameters for all configurations were first evaluated by single-wire measurements. The phase-averaged hot-wire output measured on the orifice centerline at y/D = 0.2 was utilized to calculate the characteristic velocity V_0 using Smith and Glezer's [9] definition. The details can be found in Ref. 15. The resulting stroke length, L_0/D, Reynolds number, and other parameters for representative cases are listed in Table 1.

Time- and phase-averaged measurements were carried out on cross-sectional planes at different downstream locations and also on the axial plane of symmetry. Only key results are presented with detailed contours of flowfield properties. However, the discussion draws on the entire data set. Synthetic jets from rectangular orifices are also compared with circular synthetic and steady jets at comparable momentum-flux ratios studied previously [15] in the same facility. Following Ref. 15, J is defined as $(V_{jet}/U_\infty)^2$ for the JICF, and $(V_{max}/U_\infty)^2$ for the SJCF.

The issue of an appropriate definition for jet penetration is addressed here. In Ref. 15 the peak in fundamental intensity profile was used as an indicator of jet penetration. However, this definition, based on the underlying periodicity, does not allow for a direct comparison of the SJCF and the JICF trajectories. For a JICF, traditionally the penetration has been defined based on location of peak velocity. With that definition jet trajectory has been shown to follow [20, 21],

$$y_{\max}/D = (x/D)^{0.33} J^{0.43} \quad , \tag{1}$$

where y_{max} is the distance of the location of the maximum streamwise velocity from the wall on the z = 0 plane. There have been other criteria for penetration of a JICF, e.g., based on the location of peak concentration of species [19]. The latter definition is apparently equivalent since peak concentration presumably tracks peak velocity. In a SJCF, however, the high-momentum 'cap' above the low-momentum 'dome' does not necessarily appear. Position and shape of high-momentum region depends on operating parameters. In other words, the location of the peak velocity is ill defined in a SJCF.

On the other hand, as with a JICF, the dome of low-momentum fluid is clearly distinguishable in a SJCF. Thus, the location of the minimum velocity found in the 'dome', y_{min}, appears be the logical common reference for the comparison of JICF and SJCF trajectories. The latter height is also used in correlation equations for JICF trajectory relatively far from the orifice at high velocity ratios [22,23],

$$y_{\min}/(VR \cdot h) = A\left(x/VR \cdot h\right)^B \tag{2}$$

where VR is the velocity ratio, h is the orifice height, and A and B are power law coefficients. Trajectory for the spanwise array of synthetic jets discharging from rectangular slots was found to follow this correlation [16] when h is replaced by orifice length, w. In the following, penetration depths and trajectory estimates based on y_{min} and Eq. (2) are considered. First, details of the flowfield of the SJCF are presented.

Time-averaged data for the AR = 8 orifice (L_0/D = 16.4 and J = 5.4, case 8b of Table 1) is shown in Fig. 2(a)-(c). These data are for 90 deg. pitch and 90 deg. yaw. Cross-sectional distributions of streamwise mean velocity, vorticity and turbulence intensity measured at x/D = 5 are presented. The crossflow velocity (U_∞) and orifice diameter (D) have been used for data normalization. Mean velocity contours in Fig. 2(a) exhibit a dome of low-momentum fluid pulled up from the boundary layer. The dome stretches up to about 3D in height with the minimum velocity u_{min} of about 0.79 at y_{min} = 1.58D. A counter-rotating vortex pair is seen in Fig. 2(b). Intense turbulent activity, with the peak coinciding with the center of the dome, is observed in Fig. 2(c). Corresponding data for SJCF and JICF from a round orifice at comparable momentum-flux ratio of J = 6 were provided in Ref. 15. Qualitative similarities are noted, and the main differences are described in the following. At the given J, while the mean velocity distribution of both synthetic jets exhibits just the low-momentum dome, the JICF is additionally capped by a kidney-shaped region of high-momentum fluid. The least pronounced velocity deficit ($u_{min} \approx$ 0.91) in the dome occurred with the circular SJCF, followed by the rectangular SJCF ($u_{min} \approx 0.79$) and the round JICF ($u_{min} \approx$ 0.62) jet. Peak turbulence intensity followed the same trend. The strength of the streamwise bound vortex pair was comparable between the synthetic jets but considerably stronger for the JICF. Additional vortex pair of opposite sense underneath the bound vortex pair was observed for both the SJCF and the JICF from the circular orifice.

Data corresponding to Fig. 2 for zero yaw are presented in Fig. 3. The orifice orientation strongly influences jet characteristics. The 'dome' is more than 4D high, velocity deficit has decreased ($u_{min} \approx 0.86$), and its location moved up to y_{min}/D = 3.41. Magnitudes of velocity deficit and turbulence intensity in the dome are comparable with the values obtained from circular synthetic jet. Bound vortex pair appears stronger than its yawed and circular counterparts. Jet penetration is somewhat higher than that of circular SJCF or JICF; the latter two were shown to be comparable in Ref. 15.

Only streamwise velocity contours for the case of Fig. 2 are shown in Fig. 4, for x/D = 10. Comparison with Fig. 2(a) provides an idea about the evolution of the SJCF. With increasing x/D, the dome stretches upwards. The jet penetration actually has increased fast within the first few diameters but then leveled off. The minimum velocity location, y_{min}, changes only slightly between x/D = 5 and 10. It is noteworthy that only at x/D = 0.5 (data not shown) the mean velocity field has a kidney-shaped cap over the dome. With increasing downstream distance the cap disappears and the dome becomes the distinctive characteristic of the flowfield.

For β = 90 deg., mean velocity distributions at x/D = 5 are shown in Fig. 5 for AR = 4 and 16. Figures 5(a)-(b) complement Fig. 2(a) and illustrate the effect of aspect ratio on the flowfield. Maximum velocity deficit occurs for AR = 16. It can be seen that y_{min} decreases as AR is increased from 4 to 8 but increases when AR is further increased to 16. The reversal in trend at AR = 16 remains unresolved. A possible contributor could be the effect of larger boundary layer thickness relative to the orifice width. In any case, the AR = 4 and 8 cases only are considered in the following for an examination of the trajectories.

The jet trajectories, based on y_{min} location, are shown in Fig. 6. The symbols represent the data obtained from vertical velocity profiles measured at various downstream locations on the symmetry plane. The lines are curve-fit through the data points. In Fig. 6(a) the data are shown in the usual format with distances normalized by D. In conformity with Eq. (2) the data are also shown with normalization by the product of velocity ratio and the orifice height (VRh). The latter scaling exhibits a reasonable collapse of the two data sets. Thus, the trajectories are well represented by Eq. (2).

The mean streamwise velocity contours at x/D = 5 are shown in Fig. 7 for β = 10 and 45 deg. Comparison with Figs. 2(a) and 3(a) provide a full picture of the effect of yaw on the flowfield. The low-momentum dome is tilted to the right for the intermediate values of the yaw. The tilt is more pronounced at β = 10 deg. In the latter case, traces of high-momentum cap over the dome are present. Jet penetration decreases considerably between 0 and 10 deg yaw, while the velocity deficits are comparable.

The effect of momentum-flux ratio is now explored for 90 deg yaw. Figure 8 presents streamwise velocity contours at x/D = 5 for cases 6, 9a and 8b of Table 1. Minimum velocities in the dome are approximately of the same magnitude (0.8). At low J, the low-momentum dome is connected to the boundary layer. Increasing J from 1 (Fig. 8 top) to 5.4 (Fig. 2a) results in a lifting of the dome. With further increase in J the dome completely separates and becomes a 'puff' hovering above the boundary layer. Simultaneously, the region of high-momentum fluid changes location. At J = 1, traces of kidney-shaped cap may be discernible above the dome. At higher J high-momentum fluid migrates downward on either side of the dome. At large J, the high-momentum fluid is brought underneath the separated dome.

In comparison to the AR = 8 rectangular case, circular SJCF have consistently smaller velocity deficits (0.9). Neither SJCF exhibits a topological change that was observed for the JICF with varying J in Ref. 15. The JICF was characterized by the low-momentum dome only for $J < 3$. For $J > 3$, the kidney-shaped cap appeared over the dome. Thus, with respect to this topological feature, the SJCF seem to behave like a JICF at a lower J.

Figure 9 documents jet penetration as a function of momentum-flux ratio for fixed downstream distance, x/D = 5. Data for the AR = 8 rectangular SJCF (β = 90 deg.) are compared with both SJCF and JICF from a circular orifice. Based on y_{min} the penetration of the circular and the rectangular SJCF are found comparable. However, there are differences in the rate of change with changing J. The penetration, y_{min}, for the round JICF, on the other hand, increases more rapidly with increasing J. The underlying reasons for the observed differences remain unclear.

Finally, the unsteady character of the SJCF is captured with distributions of phase-averaged properties. Phase-averaged data were acquired with the same ×-wire technique for a total of 19 phases within the cycle. Velocity contours on the plane of symmetry are shown in Figs. 10 for approximate phases of 20, 60, 100, 160, 220, 260, 300 and 340 deg. from an arbitrary reference within the cycle. These data are for the AR = 8 case with 90 deg yaw at J = 5.4. Note that two different scales have been used for the left and right columns in order to highlight the flow structures. The spatial periodicity in the flow is clearly seen. While the dimensionless stroke length is 16.4, the 'wavelength' is about $10D$. The latter corresponds to a convection speed of $0.9U_\infty$. As expected, changes in velocity magnitude (from 0.5 to 1.76) are more dramatic than those seen in time-averaged data.

Streamwise velocity contours $5D$ away from the orifice corresponding to the phases of Fig. 10 are shown in Fig. 11. Considerable changes take place depending on the phase. During the 'discharge' phases (captured on the left column) the distributions resemble those seen in time-averaged data at various J. At peak discharge conditions the high-momentum cap is clearly visible over the low-momentum dome. Changes in velocity magnitudes (from 0.52 to 1.14) are again more substantial than those found in time-averaged data. Corresponding phase-averaged streamwise vorticity were also measured but are not shown for brevity.

CONCLUSIONS

Qualitative flowfield similarity between synthetic and steady jets in crossflow is observed. However, a high-momentum 'cap' above the low-momentum 'dome', characteristic of steady jets, does not necessarily appear in the flowfield of synthetic jets. Location and shape of high-momentum region is shown to depend on the distance from the orifice, orifice pitch, yaw its orientation and momentum-flux ratio. On the other hand, the low-momentum dome is a

prominent feature in the SJCF as well as JICF. Thus, the location of the minimum velocity, y_{min}, is used for an estimate of penetration depth and comparison of synthetic and steady jet trajectories.

The increase in yaw reduces penetration height but augments the velocity deficit. Both the 'dome' and traces of high-momentum structure above it, are present for $\beta = 10$ and 45 deg, while higher velocity regions at $\beta = 0$ and 90 deg are seen on either side of the dome. Jet trajectories indicate somewhat higher penetrations for $AR = 4$. The velocity deficit is the largest both spatially and magnitude wise for $AR = 16$.

At low J, the dome is connected to the boundary layer. Increasing J lifts it and reshapes it into a 'puff' hovering above the boundary layer. Simultaneously, the regions of high-momentum fluid are redistributed. At J around 1, traces of kidney-shaped high velocity region is visible above the dome. At higher J this fluid migrates downward on either side of the dome, eventually depositing underneath the 'puff'.

Phase-averaged data show dynamic topological alterations within the cycle. Velocity data on the axial plane of symmetry exhibit periodic passage of the flow structures. While the stroke length was about $16D$ the 'wavelength' was found to be about $10D$. The latter corresponded to a convection velocity of about $0.9U_\infty$. Phase-averaged streamwise velocity contours on the cross-sectional plane at a fixed x captured the topological changes with 'discharge' and 'suction' of the cycle. During the discharge half, the changes resemble that seen in the time-averaged data at various J. Distorted and inverted kidney-shape of high-momentum fluid is initially underneath the low-momentum dome. The dome gets larger and more prominent. The high momentum fluid eventually appears as a clear kidney-shaped cap over the dome. As expected, during the suction half of the cycle the flowfield appears clean and devoid of any structures.

ACKNOWLEDGMENTS

The work was supported by NASA-Ohio Aerospace Institute (OAI) Collaborative Aerospace Research and Fellowship Program. The second author is grateful to Connecticut Space Grant College Consortium – The Experimental Program to Stimulate Competative Research (EPSCoR) Core Funding for providing support. The authors are also thankful to Dr. Gerard E. Welch of US Army Research Laboratory for valuable inputs.

REFERENCES

[1] Wallis, R. A., "The Use of Air Jets for Boundary Layer Control," Aerodynamics Research Laboratories, *Aero Note* 110, N-34736, Melbourne, Australia, January 1952.

[2] Johnston, J. P., and Nishi, M., "Vortex Generator Jets – Means for Flow Separation Control," *AIAA Journal*, **28**(6): 989-994, 1990.

[3] Compton, D. A. and Johnston, J. P., "Streamwise Vortex Production by Pitched and Skewed Jets in a Turbulent Boundary Layer," *AIAA Journal*, **30**(3): 640-647, 1992.

[4] Selby, G. V., Lin, J. C., and Howard, F. G., "Control of Low-Speed Turbulent Separated Flow Using Jet Vortex Generators," *Experiments in Fluids*, **12**: 394-400, 1992.

[5] Zhang, X., "Turbulence Measurements of a Longitudinal Vortex Generated by an Inclined Jet in a Turbulent Boundary Layer," *Journal of Fluids Engineering*, **120**: 765-771, 1998.

[6] Khan, Z. U., and Johnston, J. P., "On Vortex Generating Jets," *Int. Journal of Heat and Fluid Flow*, **21**: 506-511, 2000.

[7] Bray, T. P., "A Parametric Study of Vane and Air-Jet Vortex Generators," Ph.D. Thesis, Cranfield University, College of Aeronautics, Flow Control & Prediction Group, October 1998.

[8] Milanovic, I. M., and Zaman, K. B. M. Q., "Fluid Dynamics of Highly Pitched and Yawed Jets in Cross-Flow," *AIAA Journal*, **42**(4), 2004.

[9] Smith, B. L., and Glezer, A., "The Formation and Evolution of Synthetic Jets," *Phys. Fluids*, **10**(9): 2281-2297, 1998.

[10] Amitay, M., Smith, D. R., Kibens, V., Parekh, D. E., and Glezer, A., "Modification of the Aerodynamics Characteristics of an Unconventional Airfoil Using Synthetic Jet Actuators," *AIAA Journal*, 39 (3): 361-370, 2001.

[11] Smith, B. L., and Glezer, A., "Jet Vectoring Using Synthetic Jets," *J. Fluid Mech.*, **458**:1-34, 2002.

[12] Amitay, M., Pitt, D., Glezer, A., "Separation Control in Duct Flows," *Journal of Aircraft*, **39**(4): 616-620, 2002.

[13] Carter, J., and Soria, J., "The Evolution of Round Zero-Net-Mass-Flux Jets," *J. Fluid Mech.*, **472**: 167-200, 2002.

[14] Smith, B.L., and Swift G.W., "A Comparison Between Synthetic Jets and Continuous Jets," *Exp. Fluids*, **34**: p. 467, 2003.

[15] Zaman, K. B. M. Q., and Milanovic, I. M., "Synthetic Jets in Cross-Flow: Part 1: Round Jet," AIAA Paper 03-3714, AIAA 33rd Fluid Dynamics Conference, Orlando, FL, June 2003.

[16] Smith, D. R., "Interaction of a Synthetic Jet with a Cross-flow Boundary Layer", *AIAA J.*, **40**(11): 2277-2288, 2002.

[17] Bridges, A., and Smith, D. R., "Influence of Orifice Orientation on a Synthetic Jet-Boundary- Layer Interaction", *AIAA Journal*, **41**(12): 2394-2402, 2003.

[18] Utturkar, Y., Holman, R., Mittal, R., Carroll, B., Sheplak, M., and Cattafesta, L., "A Jet Formation Criterion for Synthetic Jet Actuators," AIAA Paper 2003-0636, 41st Aerospace Sciences Meeting and Exhibit, Reno, NV, January 2003.

[19] Gordon, M., Cater, J. E., and Soria, J., "Investigation of the Mean Passive Scalar Field in Zero-Net-Mass-Flux Jets in Cross-Flow Using Planar-Laser-Induced Fluorescence," *Physics of Fluids*, **16**(3): 794-808, 2004.

[20] Abramovich, G. N., "The Theory of Turbulent Jets," The M.I.T. Press, 1963.

[21] Zaman, K. B. M. Q., and Foss, J. K., "The Effect of Vortex Generators on a Jet in a Cross-Flow," Phys. Fluids, **9**(1):106-114, 1997.

[22] Broadwell, J. E., and Breidenthal, R. E., "Structure and Mixing of a Transverse Jet in Incompressible Flow," *Journal of Fluid Mechanics*, **148**:405-412, 1984.
[23] Hasselbrink, E., and Mungal, M., "Transverse Jet and Jet Flames. Part 1. Scaling Laws for Strong Transverse Jets," *Journal of Fluid Mechanics*, **443**:1-25, 2001.

Case	AR	A (Vrms)	L_0/D	Re	U_∞ (ft/s)	J
1	4	0.5	1.4	2,335	22.8	0.0
2	4	9.6	16.6	28,503	22.8	5.5
3	8	0.22	0.5	902	-	-
4	8	0.6	1.8	3,025	-	-
5	8	1.2	4.1	7,113	-	-
6	8	2.2	6.9	11,837	22.3	1.0
7	8	4.5	11.1	19,108	-	-
8a	8	9.6	16.4	28,132	10.5	25.5
8b	8	9.6	16.4	28,132	22.8	5.4
9a	8	15	19.6	33,758	9.0	49.9
9b	8	15	19.6	33,758	16.1	15.6
10	16	0.35	1.1	1,858	-	-
11	16	9.6	15.5	26,645	22.8	4.8

Table 1 Initial condition for different SJ configurations.

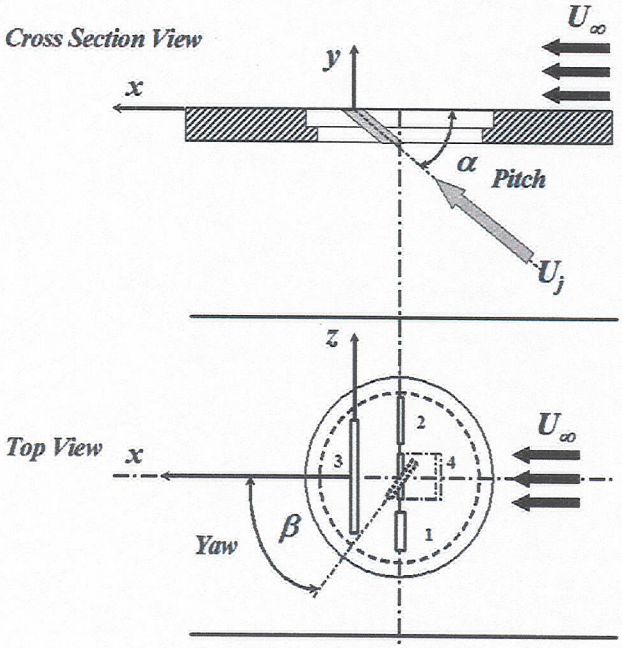

Fig. 1 Experimental setup and rectangular orifice geometries: (1) $AR = 4$, $\alpha = 90°$, (2) $AR = 8$, $\alpha = 90°$, (3) $AR = 16$, $\alpha = 90°$, (4) $AR = 8$, $\alpha = 20°$.

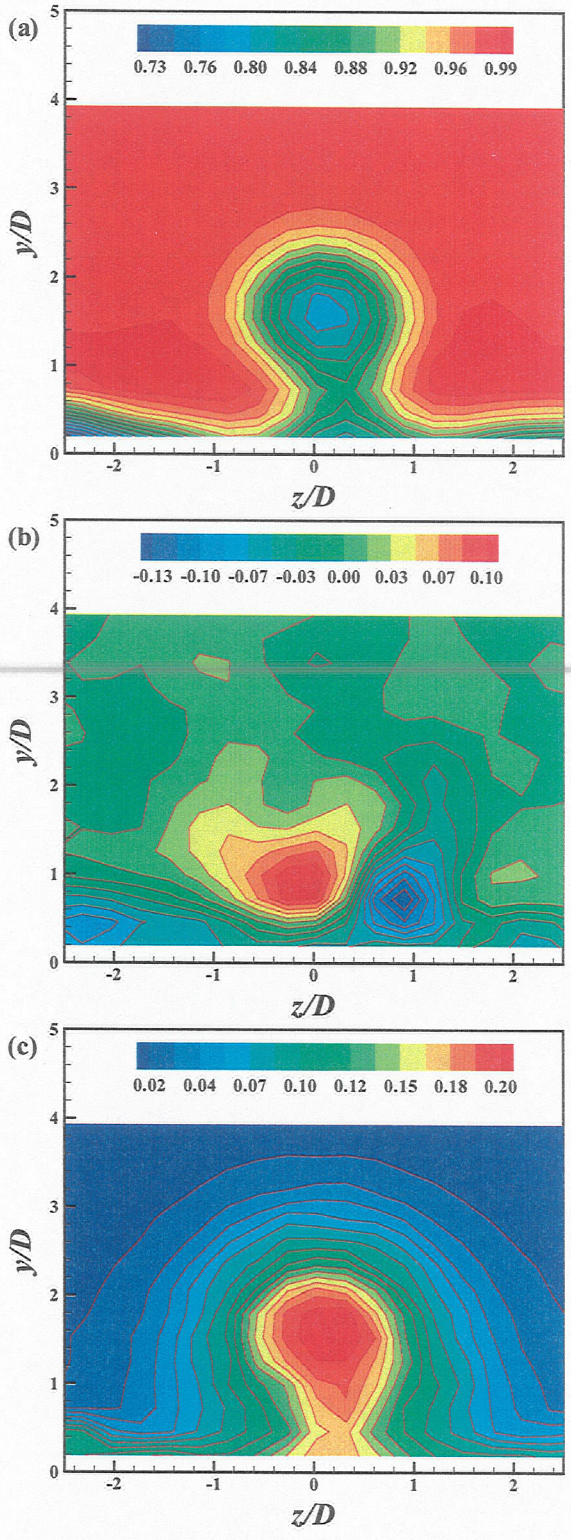

Fig. 2 Contours of streamwise (a) mean velocity, (b) vorticity and (c) turbulence intensity for $\beta = 90°$; $AR = 8$, $\alpha = 90°$, $x/D = 5$, $J = 5.4$.

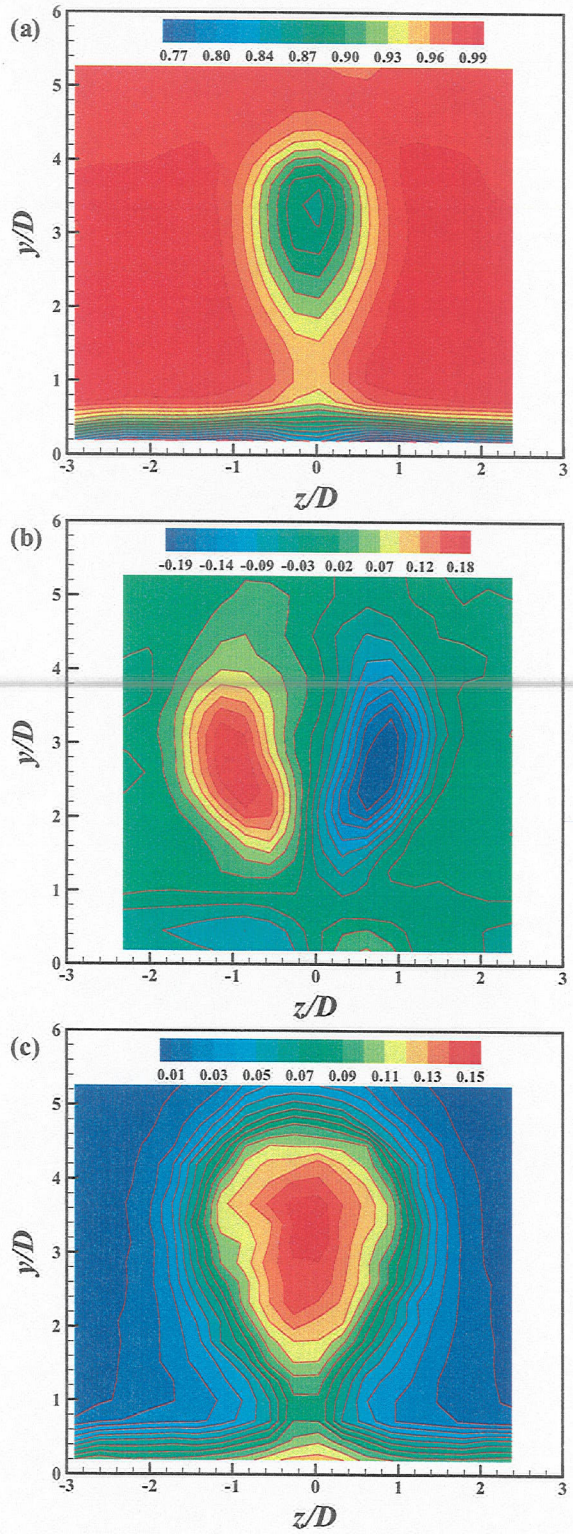

Fig. 3 Contours of streamwise (a) mean velocity, (b) vorticity and (c) turbulence intensity for $\beta = 0°$; $AR = 8$, $\alpha = 90°$, $x/D = 5$, $J = 5.4$.

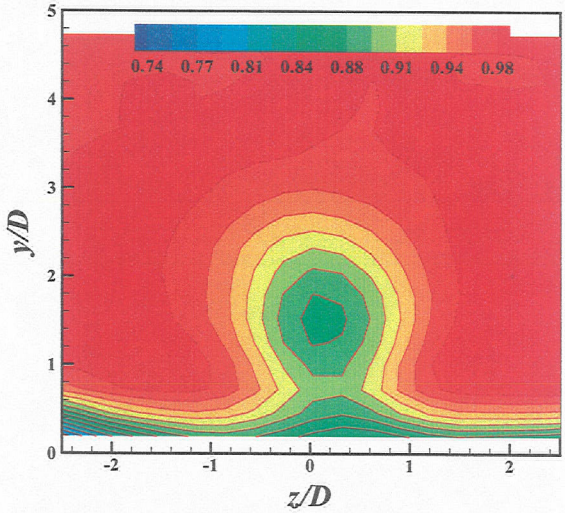

Fig. 4 Contours of streamwise mean velocity for $AR = 8$, $\alpha = 90°$, $\beta = 90°$, $x/D = 10$, $J = 5.4$.

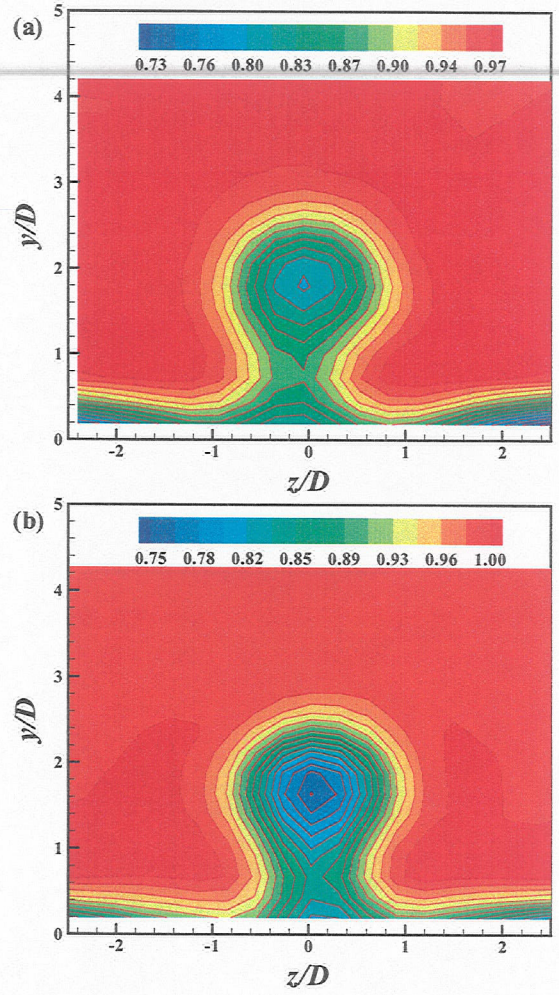

Fig. 5 Effect of aspect ratio on streamwise mean velocity for $\alpha = 90°$, $\beta = 90°$, $x/D = 5$, $J \sim 5$; (a) $AR = 4$, (b) $AR = 16$.

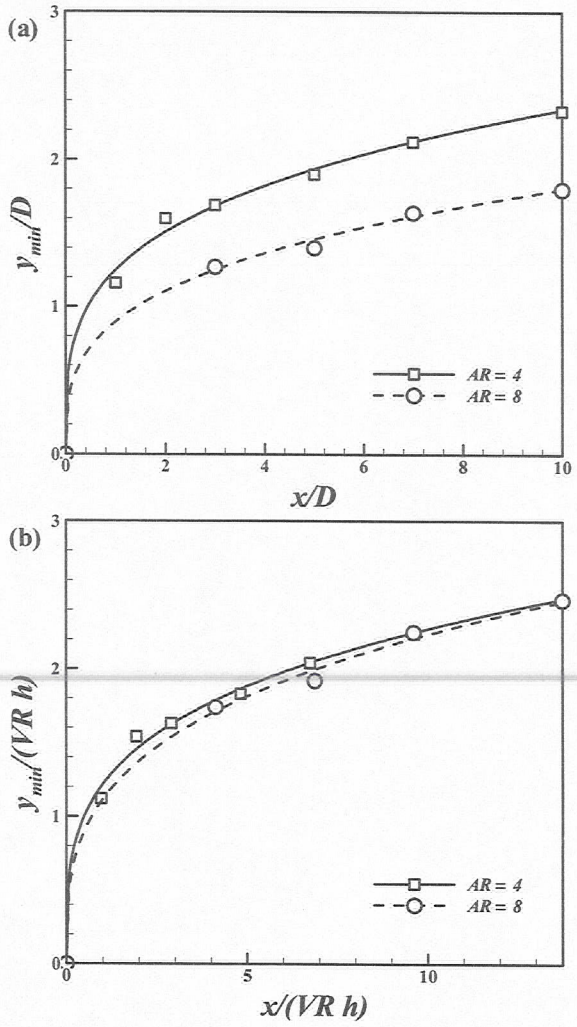

Fig. 6 SJCF Trajectories for α = 90°, β = 90°; J ~ 5; Distances normalized with (a) Equivalent diameter, (b) Product of velocity ratio and orifice height.

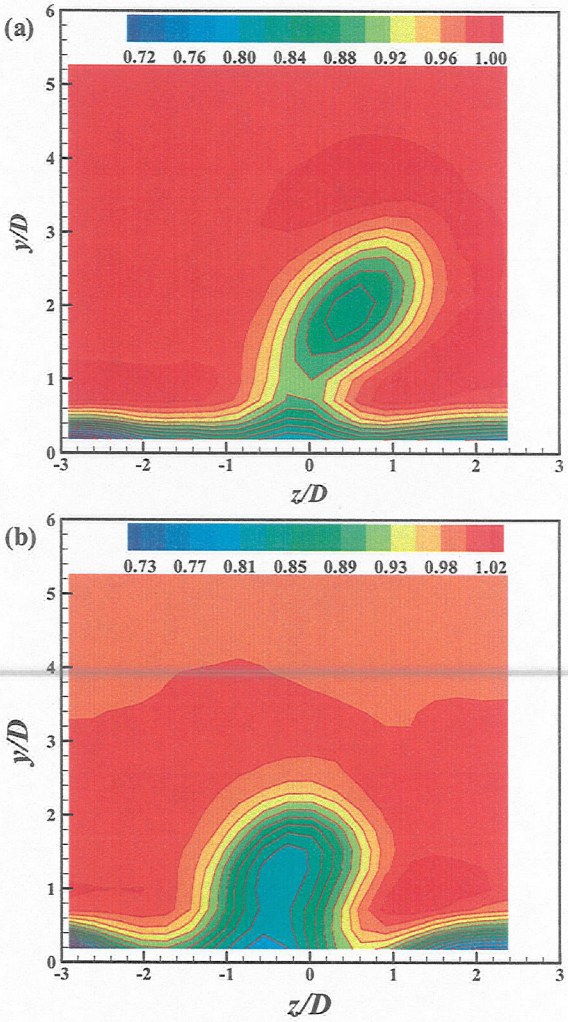

Fig. 7 Effect of yaw angle on streamwise mean velocity for AR = 8, α = 90°, x/D = 5, J ~ 5; (a) β = 10°, (b) β = 45°.

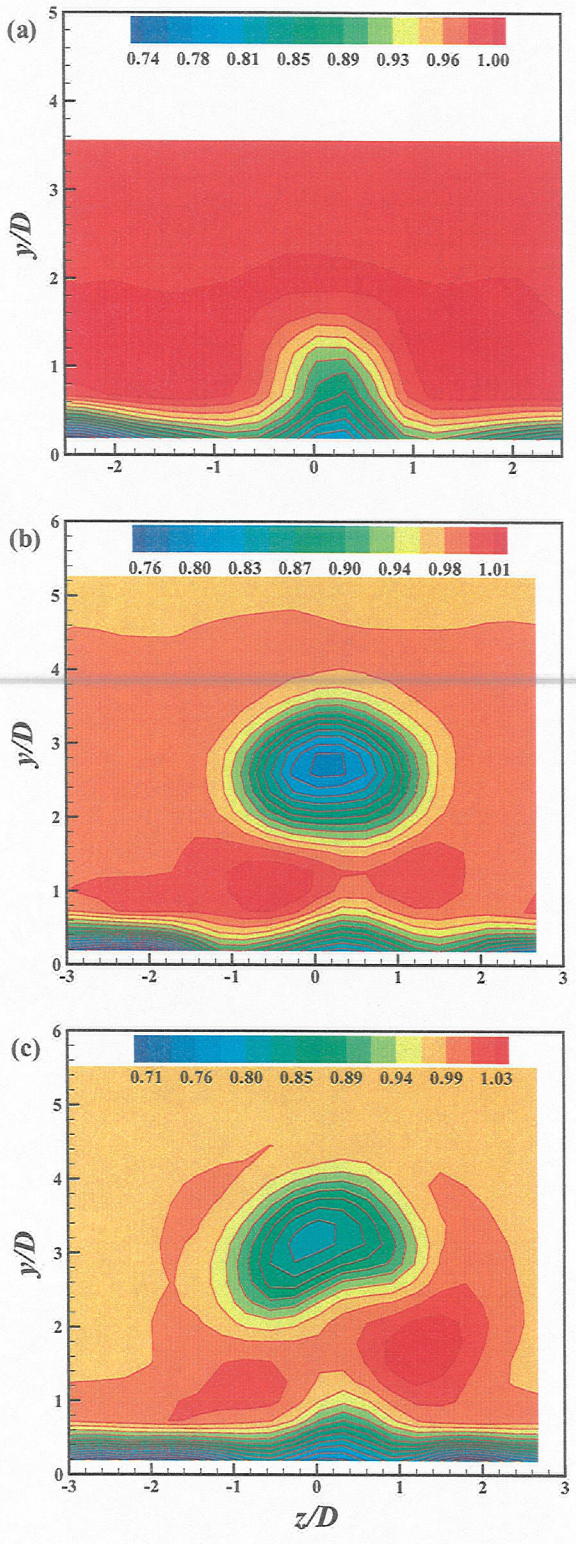

Fig. 8 Effect of momentum-flux ratio on streamwise mean velocity for $AR = 8$, $\alpha = 90°$, $\beta = 90°$, $x/D = 5$; (a) $J = 1$, (b) $J = 15.6$, (c) $J = 25.5$.

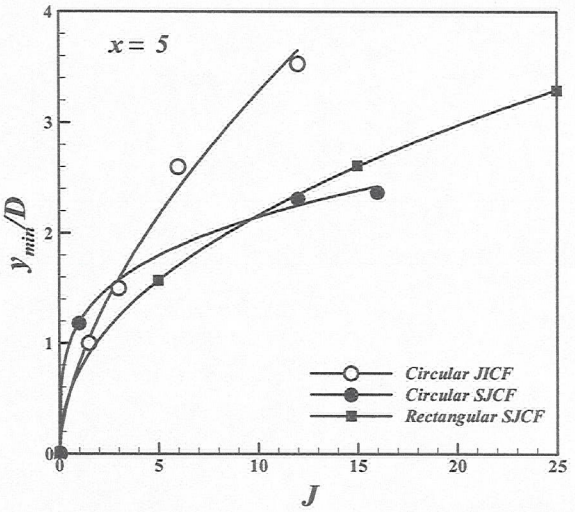

Fig. 9 Steady and synthetic jet trajectories for circular and rectangular ($AR = 8$, $\beta = 90°$) orifices; $\alpha = 90°$, $x/D = 5$.

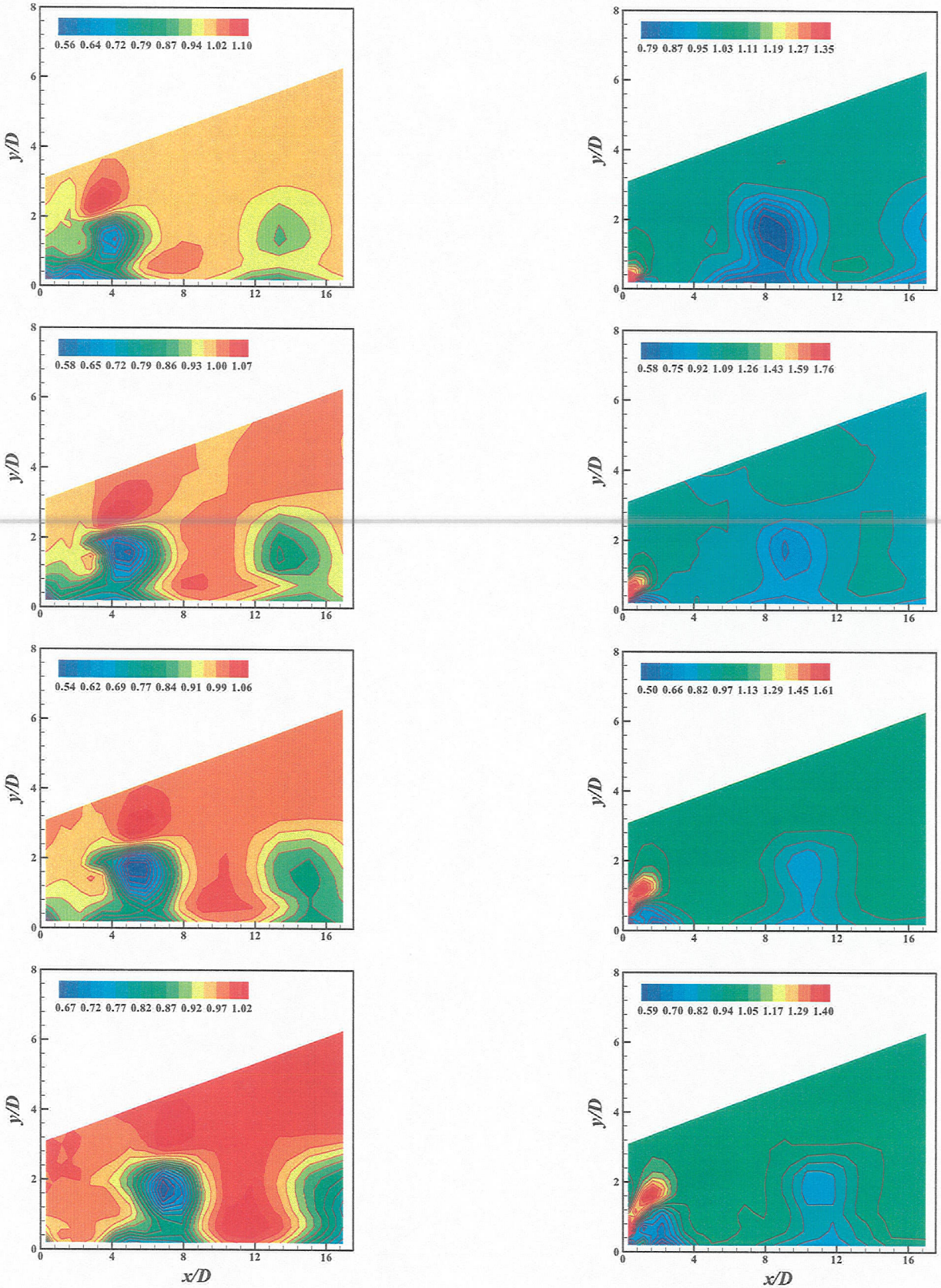

Fig. 10 Phase-averaged streamwise velocity contours on the plane of symmetry for $AR = 8$, $\alpha = 90°$, $\beta = 90°$, $J = 5.4$. The eight figures are at equally spaced phases within the excitation period.

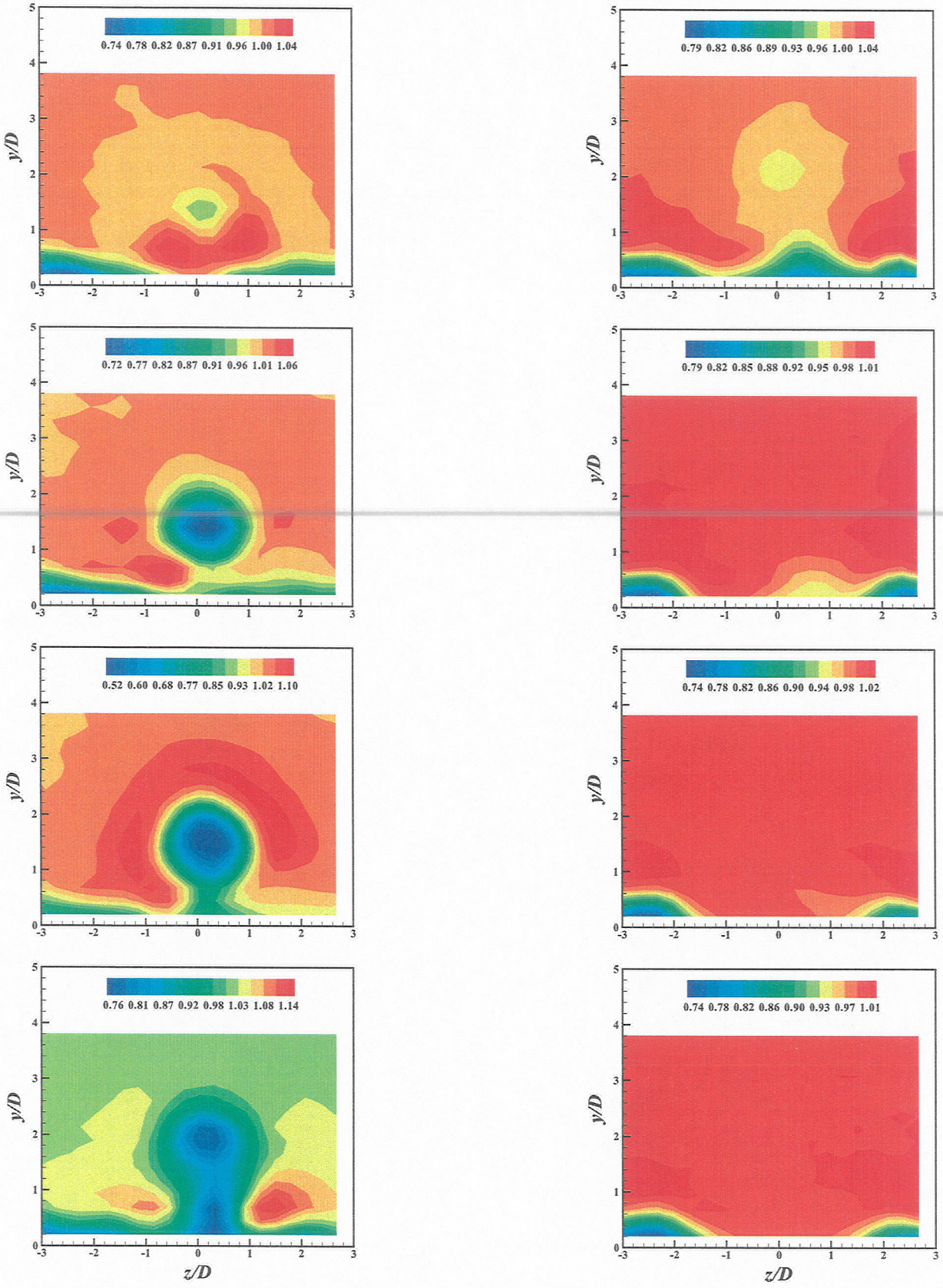

Fig. 11 Phase-averaged streamwise velocity contours for $AR = 8$, $\alpha = 90°$, $\beta = 90°$, $x/D = 5$, $J = 5.4$. The eight figures are at equally spaced phases within the excitation period.